



Quantum Chemical Computational Studies on the Structural Aspects, Spectroscopic Properties, Hirshfeld Surfaces, Donor-Acceptor Interactions and Molecular Docking of Clascosterone: A Promising Antitumor Agent

C. Karnan ^a, A. Ram Kumar ^b, S. Selvaraj ^{a,*}

^a Department of Physics, Saveetha School of Engineering, Saveetha Institute of Medical and Technical Sciences (SIMATS), Chennai, 602105, Tamil Nadu, India.

^b Department of Biotechnology, Saveetha School of Engineering, Saveetha Institute of Medical and Technical Sciences (SIMATS), Chennai, 602105, Tamil Nadu, India.

* Corresponding Author Email: sselvaphy@gmail.com

DOI: <https://doi.org/10.54392/irjmt2444>

Received: 28-04-2024; Revised: 20-06-2024; Accepted: 02-07-2024; Published: 12-07-2024



Abstract: In the present investigation, computations based on density functional theory (DFT) were employed to scrutinize the molecular configurations of clascosterone. Optimization was achieved using the DFT/B3LYP method with the 6-31G (d,p) basis set to thoroughly explore its structural and spectroscopic features. Additionally, molecular electrostatic potential (MEP) and Mulliken population analyses were conducted to comprehend the bonding characteristics and reactive sites. The Hirshfeld surface highlighted predominant H•••H interactions (71.5%), followed by O•••H interactions (25.5%). The stability of the compound was confirmed through the determination of hyperconjugative interactions using Natural Bond Orbital (NBO) analysis. Furthermore, molecular docking assessed the potential biological significance of clascosterone as an antitumor agent, targeting SMAD proteins like SMAD3 and SMAD4, resulting in binding energies of -8.22 and -8.57 kcal/mol, respectively.

Keywords: Clascosterone, DFT, NBO, MEP, Antitumor agent

1. Introduction

In recent decades, acne vulgaris has emerged as a predominant dermatological concern globally, impacting 85% of individuals aged 12 to 25. It is identified by increased skin oil production, inflammation of hair follicles, colonization by Cutibacterium, and excessive skin cell accumulation [1, 2]. Furthermore, certain hormones play a pivotal character in the growth of acne vulgaris. Testosterone is an essential hormone that undergoes metabolism by the enzyme 5-alpha-reductase to dihydrotestosterone. This process is critical in acne development since dihydrotestosterone binds to androgen receptors, thereby modulating signal cascades and inducing sebum production and sebaceous gland proliferation in both males and females [3-7]. In females, acne vulgaris has often been treated with combinations of oral contraceptives and spironolactone. However, the effectiveness of this treatment is limited due to the risk factors associated with these medications [8, 9].

Clascosterone, identified as cortexolone 17 α -propionate, represents a synthetic steroidal androgen receptor antagonist characterized by a molecular

formula denoted as C₂₄H₃₄O₅ and a molecular weight of 402.5 g/mol. structurally, clascosterone comprises a steroidal backbone consisting of four fused rings, and a propionate structure stems from the ring structure carbon atom [10-12]. Clascosterone, strives with dihydrotestosterone for binding to the androgen receptor, exerting downstream effects on pathways associated with acne development [12-14]. In addition, patients treated with clascosterone show improvement and experience reduced hair loss compared to those in the placebo group, highlighting clascosterone potential in treating androgenetic alopecia [15-17]. Furthermore, clascosterone is used to treat individuals with hidradenitis suppurative by reducing the severity and number of nodules [18].

Computational methods have become increasingly prevalent in the fields of pharmacy, pharmacology, and drug design during the last few decades, making it easier to investigate the chemical characteristics of many compounds. Among the various quantum chemical computational methodologies, Density Functional Theory (DFT) emerges as the foremost computational approach. DFT is distinguished by its precision, cost-effectiveness, adaptability, and

reliability in guessing the molecular structures of compounds [19-20]. Upon reviewing the existing literature, it was determined that theoretical spectroscopic investigations of clascosterone have not been reported yet. To address this gap and align with our research objectives, comprehensive spectroscopic and structural analyses of clascosterone were conducted, utilizing various computational techniques in quantum chemistry.

2. Computational Details

To optimize the structure and simulate vibrational frequencies, computational calculations employing quantum chemical methods were performed on the molecular assembly of clascosterone. These calculations involved the assessment of natural bond orbital (NBO), Mulliken charge distribution, and molecular electrostatic potential (MEP) surface. These calculations utilized the DFT with Becke's three parameters hybrid functional and Lee-Yang-Parr correlation (B3LYP) level of theory, implemented within the Gaussian 09 W program. The calculations were made utilizing the 6-31G (d,p) basis set without imposing any geometric constraints [21-23]. Moreover, the Gauge-Invariant Atomic Orbital (GIAO) method was employed for the computation of the isotropic chemical shifts [24, 25], and the Time-Dependent (TD) DFT approach [26, 27] was utilized to predict electronic properties using the same basis set. The outputs were visually analyzed using the Chemcraft program [28]. Crystal Explorer 3.1 was utilized to produce Hirshfeld surface and 2D fingerprint plots of clascosterone [29]. From the Protein Data Bank (PDB) of the Research Collaboratory for Structural Bioinformatics (RCSB), the 3D structures of target proteins, such as SMAD 3 (PDB

ID: 1U7F) and SMAD 4 (PDB ID: 1U7V), were obtained. Hydrogen atoms and water molecules were removed from the structures utilizing the AutoDock software [30] in order to employ Kollman charges to the designated proteins. Following this step, the interactions between the ligands and proteins were established through the utilization of PyMOL and LigPlot+ software [31, 32].

3. Results and Discussion

3.1. Optimized Geometry

The optimized structure of clascosterone is illustrated in Figure. 1, and its geometrical parameters are provided in Table 1. The simulated values were correlated with experimental values [33]. The simulated optimized bond distances for O1-C10 and O2=C22 are 1.468 and 1.214 Å, respectively, which agree with experimental values of 1.406 and 1.212 Å. The calculated bond distance of the hydroxyl (O-H) group is 0.970 Å, whereas the observed value was 0.819 Å. The optimized bond distances of C-H and C-C were computed between 1.088 to 1.102 and 1.350 to 1.574 Å, respectively, and experimental bond distances are between 1.088 to 1.102 and 0.930 to 1.043 Å. The bond angles of C10-O1-C27, C26-O3-H60, and O1-C27-O5 were simulated at 118.9°, 106.3°, and 123.7°, respectively, and experimentally observed as 117.6°, 109.4°, and 123.0°. The O-C-C and O-C-H bond angles are between 105.5 to 125.0° and 106.9 to 112.6°, while the corresponding experimental values range between 104.8-125.3° and 108.0-118.0°. Meanwhile, the bond angles of H-C-H and C-C-H were computed between 105.4 to 108.5° and 105.2 to 115.1°, respectively, with corresponding experimental values observed between 105.2-117.8° and 107.1-111.3°.

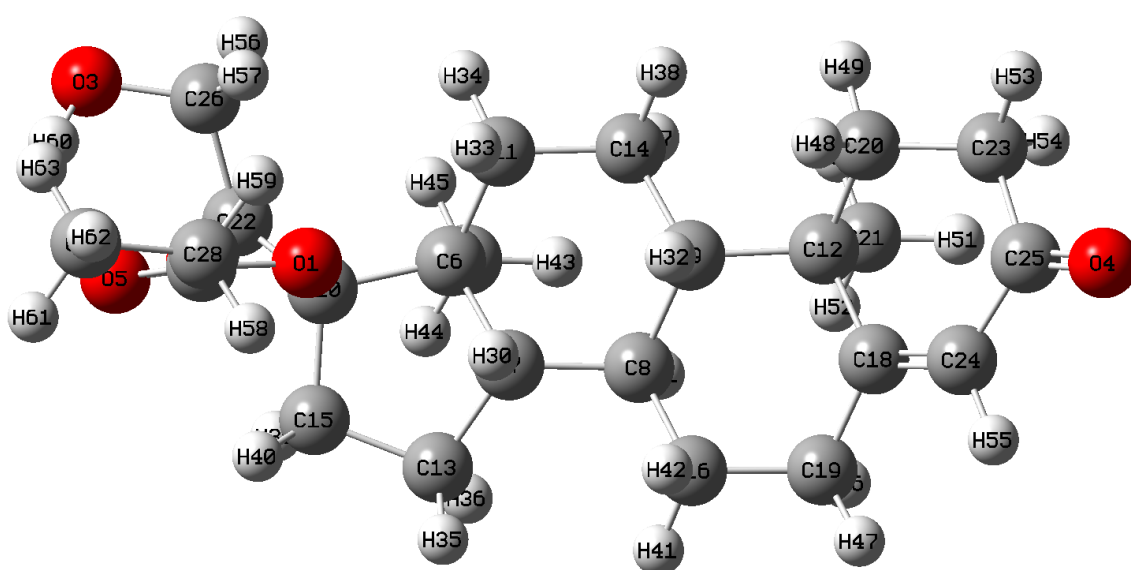


Figure 1. Optimized molecular structure of clascosterone

Table 1. Theoretical and experimental geometrical parameters (bond lengths and bond angles) of clascosterone

Bond lengths (Å)	Theoretical	Experimental ^a	Bond lengths (Å)	Theoretical	Experimental ^a
O1-C10	1.468	1.459	C15-H39	1.091	0.969
O1-C27	1.346	1.335	C15-H40	1.092	0.969
O2-C22	1.214	1.212	C16-C19	1.535	1.518
O3-C26	1.409	1.406	C16-H41	1.096	0.946
O3-H60	0.970	0.819	C16-H42	1.099	1.063
O4-C25	1.224	1.215	C17-H43	1.091	0.960
O5-C27	1.218	1.210	C17-H44	1.091	0.959
C6-C7	1.554	1.530	C17-H45	1.094	0.959
C6-C10	1.574	1.555	C18-C19	1.509	1.511
C6-C11	1.538	1.525	C18-C24	1.350	1.341
C6-C17	1.547	1.537	C19-H46	1.100	0.970
C7-C8	1.535	1.524	C19-H47	1.095	0.970
C7-C13	1.539	1.519	C20-C23	1.532	1.519
C7-H30	1.100	0.934	C20-H48	1.098	0.970
C8-C9	1.555	1.541	C20-H49	1.094	0.970
C8-C16	1.535	1.521	C21-H50	1.094	0.959
C8-H31	1.099	0.936	C21-H51	1.094	0.959
C9-C12	1.577	1.562	C21-H52	1.093	0.960
C9-C14	1.547	1.545	C22-C26	1.540	1.517
C9-H32	1.102	1.008	C23-C25	1.519	1.492
C10-C15	1.551	1.543	C23-H53	1.094	1.043
C10-C22	1.544	1.538	C23-H54	1.099	0.996
C11-C14	1.543	1.523	C24-C25	1.473	1.454
C11-H33	1.095	0.970	C24-H55	1.088	0.930
C11-H34	1.097	0.970	C26-H56	1.097	1.022
C12-C18	1.533	1.518	C26-H57	1.099	0.967
C12-C20	1.553	1.533	C27-C28	1.514	1.487
C12-C21	1.552	1.540	C28-C29	1.527	1.494
C13-C15	1.555	1.521	C28-H58	1.098	0.970
C13-H35	1.093	1.008	C28-H59	1.096	0.970
C13-H36	1.096	0.856	C29-H61	1.093	0.960
C14-H37	1.095	0.988	C29-H62	1.093	0.960
C14-H38	1.094	1.014	C29-H63	1.093	0.960
Bond angles (°)	Theoretical	Experimental ^a	Bond angles (°)	Theoretical	Experimental ^a
C10-O1-C27	118.9	117.6	C11-C14-H37	109.3	112.0
O1-C10-C6	105.5	104.8	C11-C14-H38	108.0	108.5
O1-C10-C15	109.2	110.3	H33-C11-H34	106.9	108.0
O1-C10-C22	111.1	107.1	C18-C12-C20	109.7	108.9

O1-C27-O5	123.7	123.0	C18-C12-C21	108.2	107.4
O1-C27-C28	111.3	111.5	C12-C18-C19	116.9	116.4
O2-C22-C10	120.1	119.2	C12-C18-C24	122.9	122.8
O2-C22-C26	120.1	121.4	C20-C12-C21	109.7	109.8
C26-O3-H60	106.3	109.4	C12-C20-C23	114.2	114.6
O3-C26-C22	111.7	111.6	C12-C20-H48	108.3	108.6
O3-C26-H56	106.9	118.0	C12-C20-H49	109.8	108.5
O3-C26-H57	112.6	108.0	C12-C21-H50	111.1	109.5
O4-C25-C23	122.4	121.4	C12-C21-H51	110.7	109.4
O4-C25-C24	121.9	121.9	C12-C21-H52	112.2	109.4
O5-C27-C28	125.0	125.3	C15-C13-H35	111.9	109.2
C7-C6-C10	100.0	100.7	C15-C13-H36	110.8	112.2
C7-C6-C11	108.4	108.3	C13-C15-H39	112.5	110.3
C7-C6-C17	112.7	112.1	C13-C15-H40	112.5	110.3
C6-C7-C8	113.9	113.0	H35-C13-H36	106.8	111.2
C6-C7-C13	103.9	104.3	H37-C14-H38	106.0	106.7
C6-C7-H30	105.6	101.7	H39-C15-H40	106.7	108.5
C10-C6-C11	116.9	116.5	C19-C16-H41	109.6	114.5
C10-C6-C17	108.4	108.2	C19-C16-H42	109.4	108.4
C6-C10-C15	103.7	103.7	C16-C19-C18	112.6	112.1
C6-C10-C22	113.5	111.9	C16-C19-H46	108.4	109.1
C11-C6-C17	110.2	110.4	C16-C19-H47	110.9	109.1
C6-C11-C14	111.0	110.8	H41-C16-H42	106.7	104.4
C6-C11-H33	109.3	109.4	H43-C17-H44	107.7	109.4
C6-C11-H34	111.2	109.5	H43-C17-H45	107.3	109.4
C6-C17-H43	111.3	109.4	H44-C17-H45	106.9	109.4
C6-C17-H44	112.8	109.4	C19-C18-C24	120.1	120.1
C6-C17-H45	110.7	109.4	C18-C19-H46	108.6	109.1
C8-C7-C13	119.6	119.9	C18-C19-H47	109.8	109.2
C8-C7-H30	106.1	110.7	C18-C24-C25	124.4	124.2
C7-C8-C9	109.1	109.0	C18-C24-H55	120.4	117.8
C7-C8-C16	111.5	112.9	H46-C19-H47	106.3	107.8
C7-C8-H31	108.9	107.5	C23-C20-H48	108.3	108.6
C13-C7-H30	106.7	105.2	C23-C20-H49	109.4	108.6
C7-C13-C15	104.2	105.2	C20-C23-C25	111.6	111.9
C7-C13-H35	112.3	109.6	C20-C23-H53	111.7	111.2
C7-C13-H36	110.9	108.5	C20-C23-H54	110.7	110.5
C9-C8-C16	110.1	110.0	H48-C20-H49	106.5	107.5
C9-C8-H31	109.4	107.9	H50-C21-H51	107.6	109.5
C8-C9-C12	113.8	114.0	H50-C21-H52	107.8	109.3

C8-C9-C14	112.0	111.9	H51-C21-H52	107.2	109.4
C8-C9-H32	105.3	105.9	C22-C26-H56	106.8	106.6
C16-C8-H31	107.8	109.0	C22-C26-H57	111.2	107.9
C8-C16-C19	111.4	110.9	C25-C23-H53	108.6	107.2
C8-C16-H41	110.5	109.1	C25-C23-H54	107.3	108.4
C8-C16-H42	109.2	108.7	C23-C25-C24	115.6	116.4
C12-C9-C14	113.1	112.6	H53-C23-H54	106.6	107.1
C12-C9-H32	105.2	105.6	C25-C24-H55	115.1	117.8
C9-C12-C18	108.8	110.1	H56-C26-H57	107.3	111.3
C9-C12-C20	108.6	108.8	C27-C28-C29	113.1	113.9
C9-C12-C21	111.8	111.5	C27-C28-H58	107.0	108.8
C14-C9-H32	106.6	105.8	C27-C28-H59	107.8	108.7
C9-C14-C11	113.5	113.8	C29-C28-H58	111.3	108.8
C9-C14-H37	109.9	108.1	C29-C28-H59	111.8	108.7
C9-C14-H38	109.8	107.0	C28-C29-H61	111.0	109.4
C15-C10-C22	113.4	118.2	C28-C29-H62	110.3	109.4
C10-C15-C13	107.0	106.8	C28-C29-H63	111.2	109.4
C10-C15-H39	108.6	110.3	H58-C28-H59	105.4	107.5
C10-C15-H40	109.5	110.3	H61-C29-H62	108.5	109.4
C10-C22-C26	119.6	119.2	H61-C29-H63	107.5	109.4
C14-C11-H33	109.3	109.4	H62-C29-H63	108.2	109.4
C14-C11-H34	109.0	109.5	-	-	

^a Taken from Ref. [33]

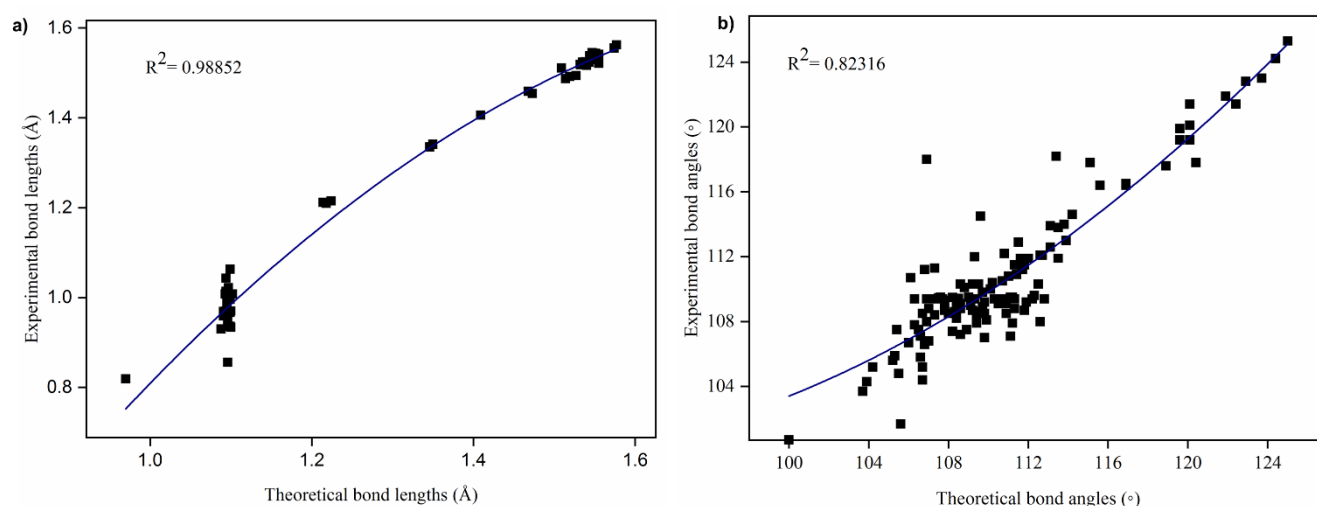


Figure. 2 (a). Correlation graph for bond lengths of clascosterone, (b) Correlation graph for bond angles of clascosterone

The bond angles of carbon atoms in C-C-C were computed between 100 to 124.4°, closely aligning with experimental values ranging between 100.7-124.2°. The bond angle of C18-C24-C25 is simulated as 124.4° and experimentally observed as 124.2°, representing a

deviation of 4° from the standard value of 120°. This discrepancy is attributed to the influence of the highly electronegative O4 atom attached to C25, resulting in a weaker bond angle compared to other carbon bond angles. The simulated values show good agreement

with experimental results, as indicated by linear coefficients (R²) of 0.98852 for bond distances and 0.82316 for bond angles, as shown in Figure. 2.

3.2. Vibrational Analysis

Clascosterone is composed of 63 atoms and exhibits 183 fundamental modes of vibrations according to (3N-6) degrees of freedom while defaulting to the C₁ point group symmetry. In the mid-IR region, the bending and stretching vibrations of O-H, C-H, C-O, C-C, C=O, CH₃, and CH₂ groups are observed. The theoretical vibrational spectra are illustrated in Figure. 3, with the corresponding wavenumbers depicted in Table 2.

3.2.1. Stretching vibrations

The optimized molecular structure of clascosterone, which includes three methyl groups, gives rise to both asymmetric and symmetric vibrations. These vibrations of the methyl groups occur at 2870 and 2980 cm⁻¹ [34]. In clascosterone, symmetric modes were simulated at 2947,

2941, 2939, 2934, and 2933 cm⁻¹, while asymmetric modes were computed at 3019, 3010, 3006, and 3002 cm⁻¹. The C-O and C=O stretching modes typically occur between 1260-1000 and 1550-1850 cm⁻¹ [35], with simulations indicating frequencies at 1737,

1712, 1705, 1197, and 1186 cm⁻¹ for these modes. The $\nu(\text{O-H})$ is influenced by chemical and physical environments, expected to fall between 3700-3550 cm⁻¹ [36], with hydroxyl stretching specifically simulated at 3617 cm⁻¹. Asymmetric and symmetric stretching vibrations of methylene groups are observed within the ranges of 3100-3000 and 3000-2900 cm⁻¹, respectively [37]. The CH₂ asymmetric and symmetric stretching were simulated between 3032-2049 and 2939-2898 cm⁻¹, respectively. In clascosterone, CH modes were computed between 3048 to 2865 cm⁻¹ [38]. Distinct and notable $\nu(\text{C-C})$ typically occur within the range of 1200-1650 cm⁻¹ [39], whereas the present study simulated $\nu(\text{C-C})$ is within the range of 1613-1453 cm⁻¹.

3.2.2. Bending vibrations

The optimized molecular structure of clascosterone includes a single hydroxyl group (O-H), leading to in-plane and out-of-plane deformations. In general, O-H in-plane and out-of-plane deformations are observed between 1330 to 1420 and 710 to 517 cm⁻¹, respectively [40]. The OH in-plane deformations were computed at 1335, 1333, and 1185 cm⁻¹, while out-of-plane deformations were computed between 736 and 517 cm⁻¹. As for the methyl group, asymmetric and symmetric deformations were anticipated to occur within the range of 1465-1440 and 1390-1370 cm⁻¹ [41].

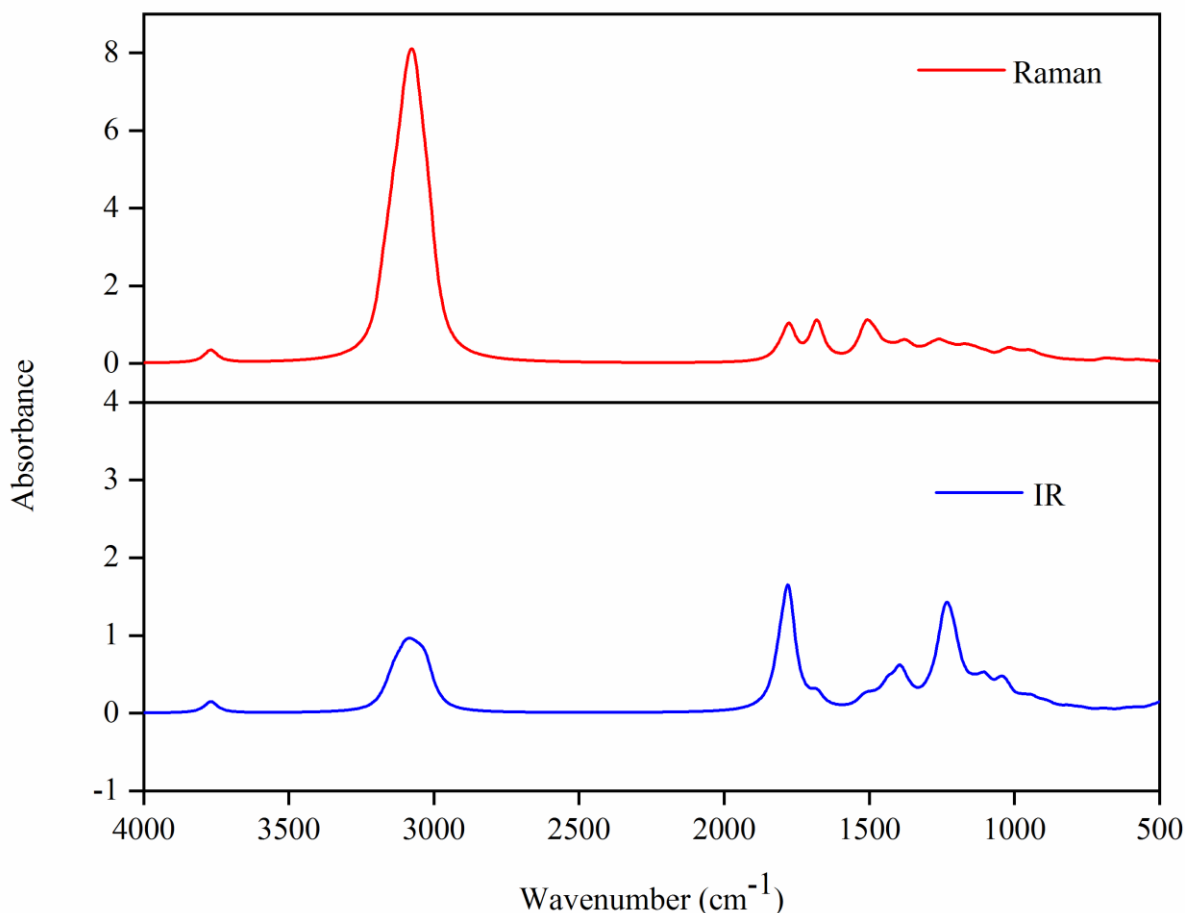


Figure 3. Simulated IR and Raman spectra of clascosterone

Table 2. Simulated IR and Raman vibrational assignments of clascosterone

Modes	Theoretical wave numbers (cm ⁻¹)				Vibrational assignments
	Unscaled	Scaled	IIR	I Raman	
1	3768	3617	49.81	42.48	u OH
2	3175	3048	11.35	115.48	u CH
3	3158	3032	17.71	50.67	u _{as} CH ₂
4	3150	3024	14.87	35.26	u _{as} CH ₂
5	3145	3019	16.31	42.01	u _{as} CH ₃
6	3137	3012	19.85	72.00	u _{as} CH ₂ in CH ₃
7	3135	3010	17.26	44.53	u _{as} CH ₃
8	3131	3006	20.78	42.91	u _{as} CH ₃
9	3127	3002	33.90	58.85	u _{as} CH ₃
10	3109	2985	22.12	128.47	u _{as} CH ₂
11	3107	2983	33.39	46.16	u _{as} CH ₂
12	3106	2982	28.49	62.73	u _{as} CH ₂
13	3097	2973	7.61	42.73	u _{as} CH ₂
14	3095	2971	44.55	93.45	u _{as} CH ₂
15	3089	2965	29.44	62.38	u _{as} CH ₂
16	3088	2964	4.27	41.21	u _{as} CH ₂
17	3085	2962	3.50	53.41	u _{as} CH ₂
18	3081	2958	39.55	105.76	u _{as} CH ₂
19	3072	2949	29.54	82.23	u _{as} CH ₂
20	3070	2947	12.51	124.30	u _s CH ₃
21	3064	2941	22.98	105.14	u _s CH ₃
22	3062	2939	18.72	80.33	u _s CH ₃ , u _s CH ₂
23	3056	2934	24.04	63.61	u _s CH ₃ , u _s CH ₂
24	3055	2933	10.86	14.67	u _s CH ₃ , u _s CH ₂
25	3050	2928	11.33	73.81	u _s CH ₂
26	3039	2917	23.92	25.66	u _s CH ₂
27	3038	2916	41.66	81.15	u _s CH ₂
28	3032	2911	40.50	67.41	u _s CH ₂ , u CH
29	3030	2909	9.05	46.59	u _s CH ₂ , u CH
30	3021	2900	7.54	9.20	u _s CH ₂ , u CH
31	3019	2898	47.72	45.02	u _s CH ₂ , u CH
32	3012	2892	10.26	117.02	u CH
33	3009	2889	3.67	31.00	u CH
34	2984	2865	7.56	17.74	u CH
35	1809	1737	124.06	17.09	u C=O

36	1783	1712	162.99	8.99	ν C=O
37	1776	1705	341.95	106.53	ν C=O
38	1680	1613	54.48	130.31	ν CC, β CH
39	1530	1469	5.08	4.65	ν CC, χ CH ₂ , δ_s CH ₃
40	1527	1466	2.05	5.00	ν CC, χ CH ₂ , δ_s CH ₃
41	1520	1459	3.76	7.54	ν CC, χ CH ₂ , δ_s CH ₃
42	1516	1455	12.19	8.88	ν CC, χ CH ₂ , δ_s CH ₃
43	1515	1454	1.77	2.91	ν CC, χ CH ₂ , δ_s CH ₃
44	1514	1453	3.31	12.59	ν CC, χ CH ₂ , δ_s CH ₃
45	1513	1452	1.77	7.21	χ CH ₂ , δ_s CH ₃
46	1511	1451	1.51	13.37	χ CH ₂ , δ_s CH ₃
47	1509	1449	6.86	20.39	δ_s CH ₃
48	1508	1448	1.98	7.05	χ CH ₂
49	1505	1445	1.71	8.63	ν CC, χ CH ₂ , δ_s CH ₃
50	1504	1444	5.42	3.87	ν CC, χ CH ₂
51	1493	1433	1.15	21.71	ν CC, χ CH ₂ , δ_s CH ₃
52	1488	1428	11.03	11.45	ν CC, χ CH ₂ , δ_s CH ₃
53	1473	1414	6.83	21.92	χ CH ₂
54	1471	1412	9.70	10.86	χ CH ₂
55	1439	1381	16.02	3.62	ν CC, β CH, δ_{as} CH ₃
56	1435	1378	43.85	3.81	ν CC, ω CH ₂
57	1434	1377	15.47	5.69	ν CC, ω CH ₂ , δ_{as} CH ₃
58	1425	1368	3.45	4.13	ν CC, β CH, ω CH ₂ , δ_{as} CH ₃
59	1417	1360	4.92	7.54	ν CC, β CH, ω CH ₂ , δ_{as} CH ₃
60	1399	1343	1.32	2.82	ν CC, β CH, ω CH ₂
61	1396	1340	88.39	1.05	ν CC, ω CH ₂ , δ_{as} CH ₃
62	1392	1336	0.95	3.46	ω CH ₂ , β CH
63	1391	1335	2.45	3.27	ω CH ₂ , β CH, β OH
64	1389	1333	37.56	8.27	ν CC, ω CH ₂ , β CH, β OH
65	1385	1329	8.10	2.92	ω CH ₂ , β CH
66	1376	1321	6.73	10.20	ω CH ₂ , β CH
67	1375	1320	1.93	8.26	ν CC, τ CH ₂ , β CH
68	1367	1312	2.50	3.74	ν CC, τ CH ₂ , β CH
69	1364	1309	13.78	5.06	τ CH ₂
70	1363	1308	1.41	10.37	ν CC, τ CH ₂ , β CH
71	1343	1289	1.12	2.96	ν CC, τ CH ₂ , β CH
72	1339	1285	6.12	2.59	ν CC, ω CH ₂ , β CH

73	1323	1270	0.67	5.94	ω CH ₂ , β CH
74	1315	1262	0.93	2.64	ω CH ₂ , β CH
75	1302	1250	1.52	7.40	τ CH ₂ , β CH
76	1293	1241	20.72	3.50	τ CH ₂ , β CH
77	1288	1236	1.94	4.93	τ CH ₂ , β CH
78	1283	1232	1.49	8.91	τ CH ₂ , δ_{as} CH ₃
79	1271	1220	2.96	3.04	τ CH ₂
80	1270	1219	4.33	7.30	τ CH ₂ , β CH
81	1259	1209	43.12	25.32	τ CH ₂ , β CH
82	1247	1197	98.13	10.49	τ CH ₂ , β CH, δ_{as} CH ₃ , u C-O
83	1235	1186	63.04	4.88	τ CH ₂ , β CH, δ_{as} CH ₃ , u C-O
84	1234	1185	169.52	4.34	τ CH ₂ , β CH, δ_{as} CH ₃ , β OH
85	1220	1171	19.63	8.66	τ CH ₂ , β OH
86	1214	1165	71.34	5.14	τ CH ₂ , β CH
87	1211	1163	26.02	5.27	τ CH ₂
88	1204	1156	62.02	2.13	τ CH ₂
89	1193	1145	29.15	3.57	τ CH ₂
90	1175	1128	10.82	25.20	τ CH ₂ , δ_{as} CH ₃
91	1160	1114	14.48	2.65	τ CH ₂ , β CH
92	1150	1104	4.69	10.01	τ CH ₂ , β CH
93	1145	1099	7.44	5.03	τ CH ₂ , β CH
94	1134	1089	28.29	9.57	τ CH ₂ , β CH
95	1128	1083	7.17	4.04	τ CH ₂ , β CH
96	1119	1074	5.73	1.47	τ CH ₂ , β CH
97	1110	1066	2.81	0.62	τ CH ₂ , δ_{as} CH ₃
98	1106	1062	14.96	1.05	δ_{as} CH ₃
99	1101	1057	64.44	13.32	τ CH ₂ , δ_{as} CH ₃ , β CH
100	1093	1049	4.08	1.61	τ CH ₂ , β CH
101	1083	1040	7.81	1.94	τ CH ₂ , β CH
102	1067	1024	7.52	1.19	ρ CH ₂ , β CH
103	1052	1010	14.01	2.98	ρ CH ₂ , β CH
104	1046	1004	44.80	0.58	ρ CH ₂ , β CH
105	1037	996	13.39	7.86	ρ CH ₂ , γ CH
106	1031	990	13.65	0.67	ρ CH ₂ , γ CH, δ_{as} CH ₃
107	1027	986	23.66	2.38	ρ CH ₂ , γ CH, δ_{as} CH ₃
108	1020	979	9.93	4.50	ρ CH ₂ , δ_{as} CH ₃
109	1016	975	4.43	20.66	ω CH ₂ , γ CH

110	996	956	2.41	2.14	ρ CH ₂ , γ CH
111	991	951	4.42	6.68	ρ CH ₂ , γ CH
112	977	938	3.39	3.25	ρ CH ₂ , γ CH
113	972	933	13.49	0.58	ρ CH ₂ , γ CH, δ_{as} CH ₃
114	958	920	10.01	13.72	γ CH, δ_{as} CH ₃
115	944	906	2.91	2.12	γ CH, δ_{as} CH ₃
116	940	902	24.56	10.93	γ CH, δ_{as} CH ₃
117	928	891	3.11	3.98	ρ CH ₂ , δ CH, δ_{as} CH ₃
118	924	887	3.91	3.21	τ CH ₂ , γ CH
119	908	872	3.52	3.68	τ CH ₂ , γ CH
120	898	862	13.96	2.75	ρ CH ₂ , γ CH
121	879	844	12.37	4.16	ρ CH ₂ , γ CH, δ_{as} CH ₃
122	867	832	2.27	3.58	τ CH ₂ , δ_{as} CH ₃
123	847	813	3.01	1.84	τ CH ₂ , δ_{as} CH ₃
124	836	803	0.93	1.64	τ CH ₂
125	818	785	1.03	1.53	ρ CH ₂
126	817	784	8.10	0.63	ρ CH ₂ , δ_{as} CH ₃
127	807	775	4.63	2.04	ρ CH ₂ , δ_{as} CH ₃
128	787	756	3.98	1.57	τ CH ₂ , γ CH
129	767	736	7.73	3.36	τ CH ₂ , γ OH
130	750	720	2.45	0.65	τ CH ₂ , γ CH
131	704	676	2.41	3.50	ρ CH ₂ , γ CH
132	693	665	4.69	3.24	τ CH ₂ , γ CH, δ_{as} CH ₃
133	679	652	3.73	5.65	ρ CH ₂ , δ_{as} CH ₃
134	663	636	0.05	3.14	ρ CH ₂ , γ OH
135	638	612	1.41	5.47	ρ CH ₂ , δ CH
136	317	304	8.71	1.42	ρ CH ₂ , δ CH
137	578	555	5.16	2.81	ρ CH ₂ , δ CH, γ OH
138	574	539	5.51	3.20	ρ CH ₂ , δ CH, γ OH
139	566	543	0.87	2.55	ρ CH ₂ , δ CH, γ OH
140	540	518	0.83	0.22	ρ CH ₂ , δ_{as} CH ₃
141	539	517	0.37	2.53	ρ CH ₂ , δ CH, γ OH
142	524	503	10.54	1.38	ρ CH ₂ , δ CH
143	514	493	3.80	0.47	ρ CH ₂ , δ CH
144	489	469	0.93	2.21	ρ CH ₂
145	463	444	10.00	0.76	ρ CH ₂
146	462	443	79.80	2.03	δ OH
147	443	425	3.17	0.88	ρ CH ₂

148	439	421	0.34	0.66	ρ CH ₂ , δ CH
149	419	402	0.02	0.99	ρ CH ₂ , δ CH, δ_{as} CH ₃
150	399	383	2.08	2.58	ρ CH ₂ , δ CH
151	383	367	1.14	0.90	ρ CH ₂
152	374	359	10.67	2.83	ρ CH ₂ , δ CH
153	359	344	2.09	2.13	ρ CH ₂
154	349	335	2.61	2.51	ρ CH ₂ , δ CH, δ OH, δ_{as} CH ₃
155	328	315	3.20	1.13	ρ CH ₂
156	325	312	2.19	1.03	ρ CH ₂
157	297	285	7.87	0.80	ρ CH ₂ , δ CH, δ OH
158	290	278	5.53	0.58	ρ CH ₂ , δ OH
159	283	272	0.74	1.46	ρ CH ₂ , δ OH
160	278	267	4.10	0.78	ρ CH ₂ , δ CH, δ OH, δ_{as} CH ₃
161	272	261	0.21	0.64	δ OH, δ_{as} CH ₃
162	253	243	2.02	0.82	ρ CH ₂ , δ CH, δ OH, δ_{as} CH ₃
163	246	236	4.54	1.59	ρ CH ₂ , δ CH, δ OH, δ_{as} CH ₃
164	236	227	0.10	0.91	ρ CH ₂ , δ_{as} CH ₃
165	226	217	0.16	0.48	δ_s CH ₃
166	215	206	0.37	0.71	δ_s CH ₃
167	208	200	0.12	0.56	δ_s CH ₃
168	201	193	0.16	0.66	δ_s CH ₃
169	177	170	1.49	0.46	δ_s CH ₃ , ρ CH ₂
170	170	163	1.58	1.55	δ_s CH ₃ , ρ CH ₂ , δ CO
171	156	150	1.41	0.60	δ_s CH ₃ , ρ CH ₂ , δ CO, δ CH
172	148	142	0.51	1.17	δ_s CH ₃ , ρ CH ₂ , δ CH
173	142	136	0.99	0.56	δ_s CH ₃ , ρ CH ₂ , δ CH, δ OH
174	114	109	2.88	0.31	δ_s CH ₃ , ρ CH ₂ , δ CH, δ CO
175	110	106	4.60	0.24	ρ CH ₂ , δ OH
176	95	91	0.69	0.37	ρ CH ₂ , δ CO
177	80	77	0.02	0.28	Ring vibration
178	69	66	0.07	0.71	Ring vibration
179	53	51	1.06	0.50	Ring vibration
180	47	45	0.32	0.09	Ring vibration
181	42	40	1.92	0.21	Ring vibration
182	33	32	0.79	0.87	Ring vibration
183	25	24	2.60	2.21	Ring vibration

ν_s - symmetric stretching; ν_{as} - asymmetric stretching; δ - bending / deformation; β - in-plane bending; γ - out-of-plane bending; χ - scissoring; ω - wagging; τ - twist; ρ - rocking

Scaling factor 0.96 for all vibrations

The asymmetric and symmetric deformations were computed within the range of 1469-1428 and 1381-1340 cm^{-1} . Out-of-plane and in-plane deformations of C-H typically occur between 1000-750 and 1450-1000 cm^{-1} [42]. The calculated C-H in-plane and out-of-plane deformations are observed between 1613-1004 and 996-665 cm^{-1} . CH_2 deformations out-of-plane (twisting and wagging) and in-plane (rocking and scissoring) were simulated below 1500 cm^{-1} .

3.3. Chemical Shift

The simulated chemical shifts of hydrogen and carbon atoms are presented in Table 3, while the atom numbering is arranged as per Figure. 1. In general, aliphatic compounds were detected up to 70 ppm for carbon atoms and 4 ppm for hydrogen atoms [43]. In this study, the chemical shifts of methyl (CH_3) carbons C_{17} , C_{29} , and C_{21} were calculated as 7.83, 1.59, and 9.68 ppm, respectively. Methyl group carbons exhibit a lower chemical shift than other carbons due to electron-donating hydrogens, resulting in more substantial shielding of the nuclear spins. The chemical shifts of C_{22} , C_{25} , and C_{27} of $\text{C}=\text{O}$ were computed at 198.19, 183.09, and 168.50 ppm, respectively. These carbons demonstrate higher chemical shifts than other functional group carbons due to the effect of highly electronegative oxygen. This decreased electron density around the carbon nucleus weakens the shielding of the nuclear spins, causing the carbon atoms in the keto group to

experience a higher effective magnetic field. The C_{26} attached with the O-H group was also simulated at 54.64 ppm. Methylene and methine group carbons were simulated between 15.33-30.59 ppm and 29.99-112.14 ppm, respectively. Within clascosterone, the chemical shifts of the hydroxyl (O-H) proton H_{60} are observed at 3.14 ppm and the methine (C-H) protons H_{55} , H_{31} , H_{32} , and H_{30} are simulated within the range of 5.81, 1.94, 1.12 and 2.11 ppm, respectively. Notably, the methine proton H_{55} experiences an increased chemical shift related to the other methine protons due to the neighbouring high electronegative O_4 , which deshielding the electrons from H_{55} . The protons attached to methylene groups are theoretically simulated between 1.28 to 3.78 ppm.

3.4. Electronic Properties

Table 4 displays the simulated excitation energies, wavelengths, oscillator strengths, and major contributions of clascosterone, while the corresponding electronic spectrum in the gas phase is depicted in Fig. 4. The simulated electronic spectrum reveals three bands, ranging from sharp to weak, observed at 252, 317, and 354 nm. For the transition with a wavelength of 354 nm and an excitation energy of 3.49 eV, the oscillator strength is 0.0002. 98% of this transition is made up of the largest contribution, which comes from the lowest unoccupied molecular orbital (LUMO) to the highest occupied molecular orbital (HOMO).

Table 3. Simulated chemical shift values (all values in ppm) of clascosterone

Atoms	Chemical shifts	Atoms	Chemical shifts	Atoms	Chemical shifts
Carbon chemical shifts					
C_6	42.88	C_{14}	15.33	C_{22}	198.19
C_7	46.80	C_{15}	27.12	C_{23}	26.28
C_8	29.99	C_{16}	26.28	C_{24}	112.14
C_9	48.13	C_{17}	7.83	C_{25}	183.09
C_{10}	95.73	C_{18}	152.57	C_{26}	54.64
C_{11}	25.64	C_{19}	26.80	C_{27}	168.50
C_{12}	34.55	C_{20}	30.59	C_{28}	20.68
C_{13}	18.72	C_{21}	9.68	C_{29}	1.59
Proton chemical shifts					
H_{30}	2.11	H_{42}	1.28	H_{53}	2.16
H_{31}	1.94	H_{43}	1.33	H_{54}	2.55
H_{32}	1.12	H_{44}	1.11	H_{55}	5.81
H_{33}	2.20	H_{45}	0.20	H_{56}	3.65
H_{34}	1.42	H_{46}	2.64	H_{57}	4.24
H_{35}	1.84	H_{47}	2.23	H_{58}	2.53

H ₃₆	1.58	H ₄₈	1.78	H ₅₉	2.71
H ₃₇	1.64	H ₄₉	2.03	H ₆₀	3.14
H ₃₈	1.72	H ₅₀	1.18	H ₆₁	1.52
H ₃₉	3.78	H ₅₁	1.43	H ₆₂	0.98
H ₄₀	1.67	H ₅₂	1.57	H ₆₃	1.33
H ₄₁	1.97	-	-	-	-

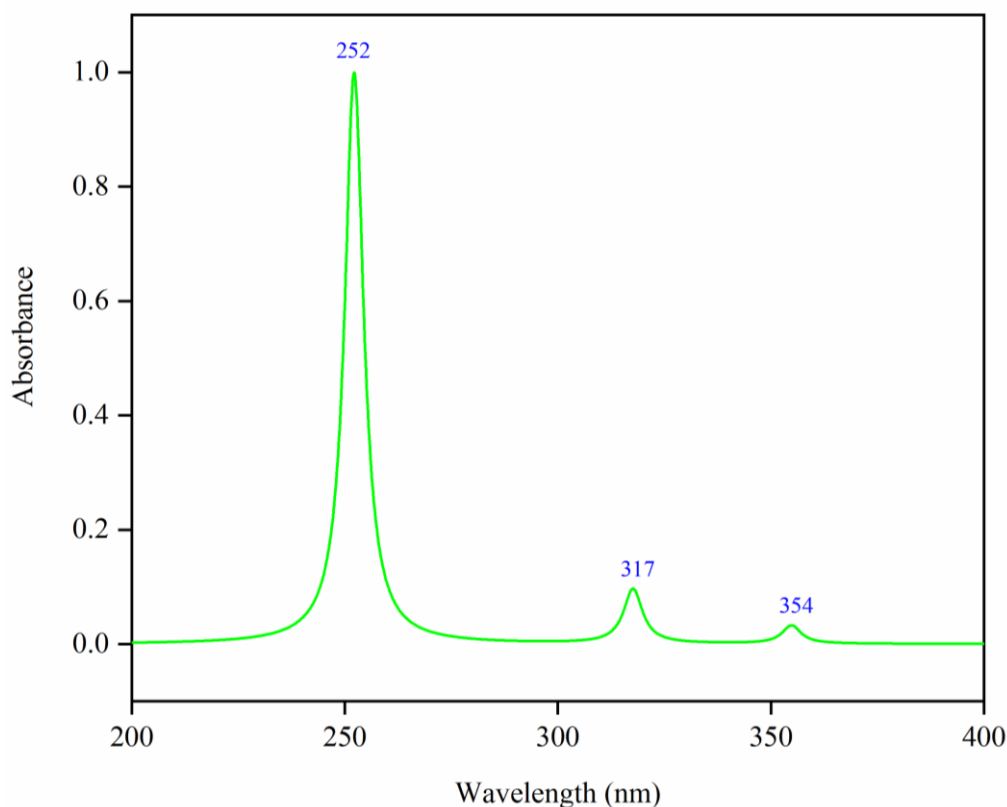


Figure 4. Theoretical electronic spectra of clascosterone

Table 4. Calculated wavelengths (λ), excitation energies (E), oscillator strengths (f) and significant contributions of clascosterone in the gas phase

λ (nm)	E (eV)	f	Major contributions	Minor contributions
354	3.49	0.0002	HOMO→LUMO (98%)	-
317	3.90	0.0006	HOMO-1→LUMO+1 (92%)	HOMO-3→LUMO+1 (4%)
252	4.91	0.0063	HOMO-1→LUMO (99%)	-

The transition with a wavelength of 317 nm and an oscillator strength of 0.0006 has an excitation energy of 3.90 eV. Here, the significant contribution is from the HOMO-1 to the LUMO+1, which constitutes 92% of the transition. Also, a minor contribution of 4% is from the HOMO-3 to the LUMO+1. Lastly, the transition with a wavelength of 252 nm and an excitation energy of 4.91 eV exhibits an oscillator strength of 0.0063. The major contribution arises from the HOMO-1 to the LUMO, accounting for 99% of the transition. The frontier

molecular orbital (FMO) map distinguishes positive and negative regions within the molecule using red and green, respectively. Energy gap values and other parameters in the gas phase are listed in Table 5 and graphically depicted in Figure 5. Additionally, Figure 6 displays a density of states (DOS) spectrum representing the energy gap of clascosterone, measured at 5.018 eV, with occupied and unoccupied orbitals represented in green and red.

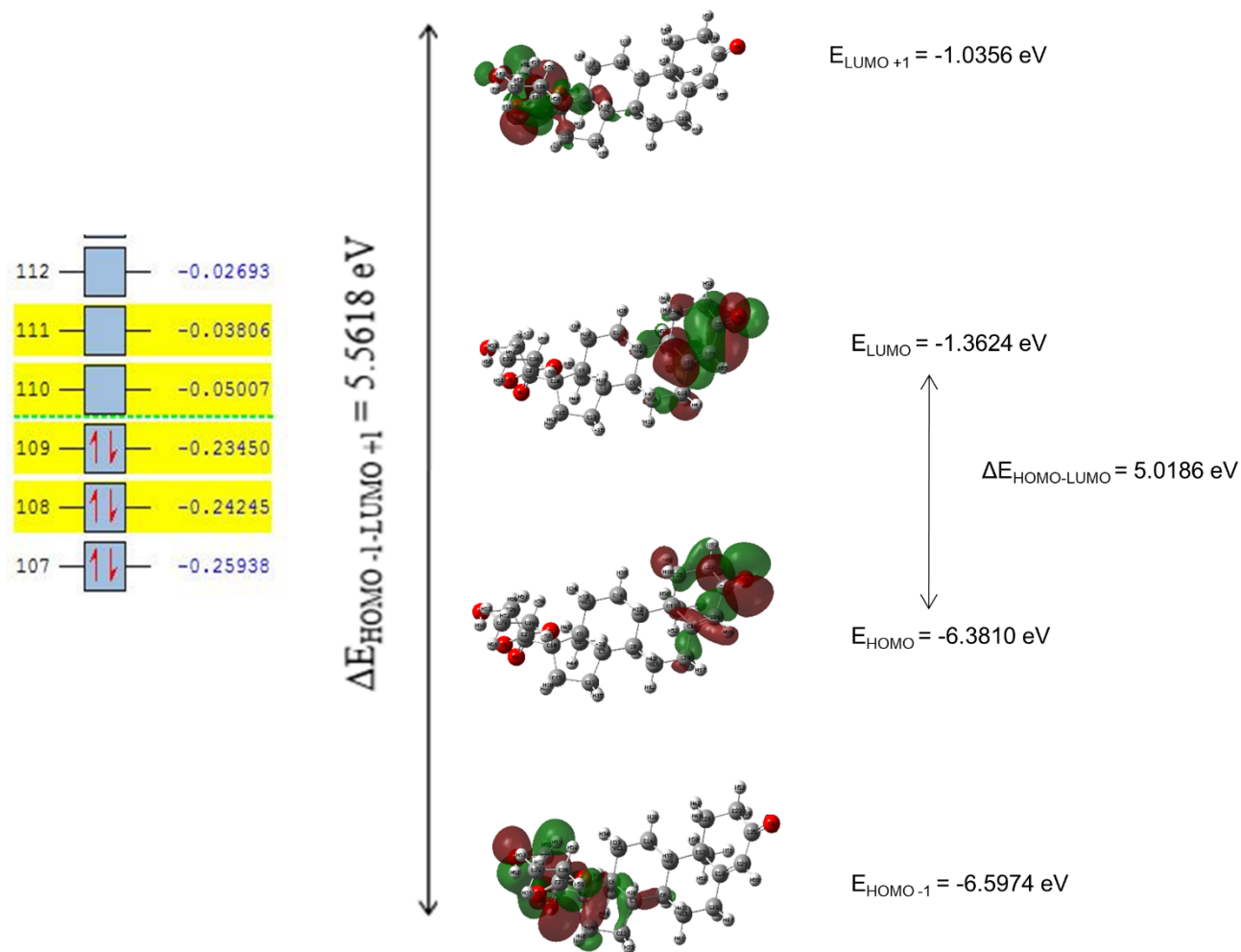


Figure 5. Simulated HOMO-LUMO energy gap of clascosterone in the gas phase

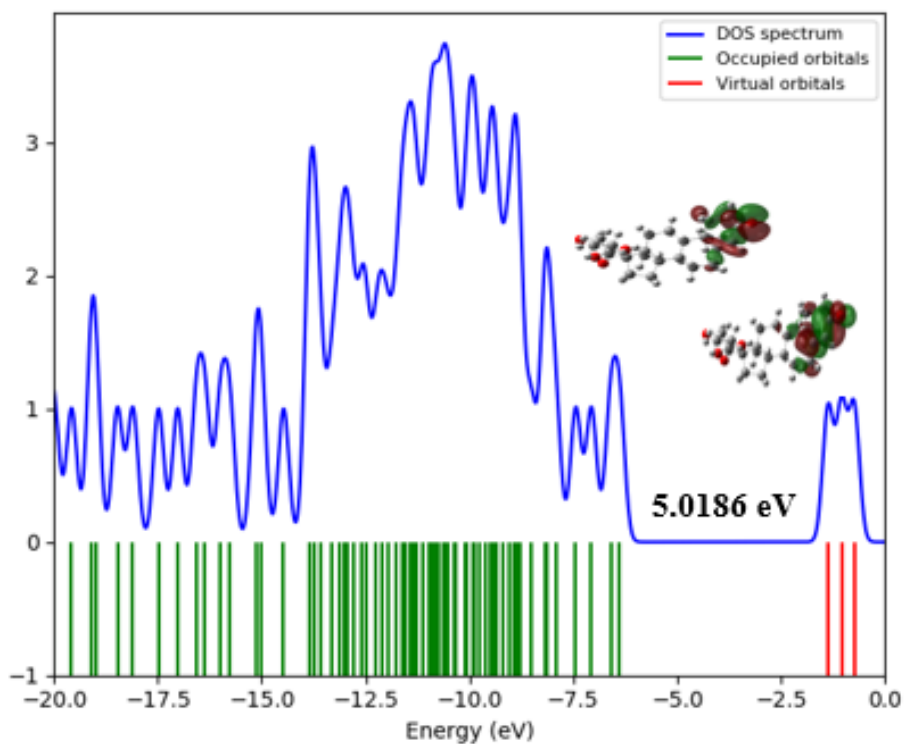


Figure 6. Simulated DOS spectrum of clascosterone in the gas phase

Table 5. Frontier molecular orbital parameters of clascosterone in the gas phase

Parameters	Formula	Gas
E_{HOMO} (eV)	-	-6.38116
E_{LUMO} (eV)	-	-1.36249
$E_{\text{HOMO-LUMO}}$ gap(eV)	-	5.01867
Ionization potential (I)	$-E_{\text{HOMO}}$	6.38116
Electron affinity (A)	$-E_{\text{LUMO}}$	1.36249
Electronegativity (χ)	$(I+A)/2$	3.87182
Chemical potential (μ)	$-\chi$	-3.87182
Chemical hardness (η)	$I-A$	5.01867
Chemical softness (s)	$1/2\eta$	0.09962
Global Electrophilicity (ω)	$\mu^2/2\eta$	1.49352
Maximum electron charge (ΔN_{max})	$-(\mu/\eta)$	0.77148

3.5. Hirshfeld Analysis

Hirshfeld surface (HS) analysis enables the examination of inter and intramolecular interactions, hydrogen bonds, and compound surfaces. HS studies were conducted and 2D fingerprint images were generated for clascosterone, as depicted in Figure. 7. These studies were based on the Crystallographic Information File (CIF) deposited by Fiorella Meneghetti [44] in the Cambridge Crystallographic Data Centre (CCDC). The d_{norm} indicates that red and blue regions denote shorter and larger van der Waals radii, respectively, with surface values from -0.6446 (red) to 1.6460 (blue), while the dark red surfaces represent visible hydrogen bonding contacts. Additionally, the colors blue and red in the shape index represent " π - π " interactions, offering insights into curvature. The 2D fingerprint plots indicate that the strong interaction primarily stems from $\text{H}\cdots\text{H}$ (71.5%), with other significant contributions from $\text{O}\cdots\text{H} / \text{H}\cdots\text{O}$ (25.5%), and weak interactions from $\text{H}\cdots\text{C} / \text{C}\cdots\text{H}$ (2.7%) and $\text{O}\cdots\text{O}$ (0.3%).

3.6. Natural Bond Orbital (NBO)

The natural bond orbital (NBO) analysis of clascosterone, including intermolecular and intramolecular interactions, charge transfers, and contributions to stabilization, is presented in Table 6. The electron donation process from O_1 to the anti-bonding $\text{O}_5\text{-C}_{27}$ via the $\text{L}(2)\rightarrow\pi^*$ transition accounts for the majority of the interaction energy in the current study, yielding an intramolecular stabilisation energy of 46.53 kJ/mol. This is followed by the second maximum contribution, arising from O_5 to the anti-bonding $\text{O}_1\text{-C}_{27}$, with the transition of $\text{L}(2)\rightarrow\sigma^*$, which is 29.52 kJ/mol. $\text{L}(2)\rightarrow\sigma^*$ interactions were observed between electron donor oxygen atoms O_5 , O_4 , and O_2 , and acceptor atoms $\text{C}_{27}\text{-C}_{28}$, $\text{C}_{24}\text{-C}_{25}$, $\text{C}_{25}\text{-C}_{23}$, $\text{C}_{22}\text{-C}_{26}$, and $\text{C}_{10}\text{-C}_{22}$, resulting

in stabilizing energies of 17.43, 18.22, 20.12, 19.76, and 19.85 kJ/mol, respectively. Additionally, a $\pi\rightarrow\pi^*$ transition from $\text{C}_{18}\text{-C}_{24}$ to the natural bond $\text{O}_4\text{-C}_{25}$ was identified, with a stabilizing energy of 21.77 kJ/mol.

3.7. Mulliken Population Analysis

Mulliken charges play a vital role in quantum chemical calculations, providing insights into molecular properties like dipole moment, charge displacement, polarizability, and identifying electrophilic and nucleophilic sites [45]. In this study, the Mulliken charge distributions of clascosterone were presented in Table 7 and visually depicted in Figure. 8. In clascosterone, all hydrogen and oxygen atoms have net negative and positive charges, respectively. Carbon atoms C_6 (0.003544e), C_{10} (0.206161e), C_{18} (0.149161e), C_{25} (0.42383e), C_{26} (0.040861e), and C_{27} (0.638068e) exhibit net positive charges, with carbon atom C_{27} showing a higher positive value due to electronegative atoms on both adjacent sides. On the other hand, carbon atoms C_7 (-0.04823e), C_8 (-0.06939e), C_9 (-0.05355e), C_{11} (-0.18447e), C_{12} (-0.01108e), C_{13} (-0.2103e), C_{14} (-0.19973e), C_{15} (-0.19778e), C_{16} (-0.18031e), C_{17} (-0.3299e), C_{19} (-0.24344e), C_{20} (-0.19738e), and C_{21} (-0.31777e) have net negative charges. Notably, carbon atom C_{17} exhibits higher negativity due to the influence of the adjacent keto group ($\text{C}=\text{O}$).

3.8. Molecular Electrostatic Potential Surface

Molecular electrostatic potential (MEP) surface is employed to differentiate electron-deficient and electron-rich regions in molecular structures, depicted through various colors on the map ranging from -6.175×10^{-2} e.s.u to 6.175×10^{-2} e.s.u (Figure. 9). The regions with high electron density (electrophilic reactivity), low electron density (nucleophilic reactivity), and neutral

potential, respectively, are the susceptible colour regions, which include red, blue, and green. In both the hydroxyl (OH) and carbonyl (C=O) groups, clascosterone displays a red zone above the oxygen atom, which suggests electron electron-rich site and possible locations for electrophilic attack, according to the MEP map. On the other hand, low electron density

and possible locations for nucleophilic reactivity are indicated by the blue zone around the hydrogen in the cyclic ring, as well as in the methyl (CH₃) and methylene (CH₂) groups. These findings are consistent with the Mulliken population analysis results that were previously discussed.

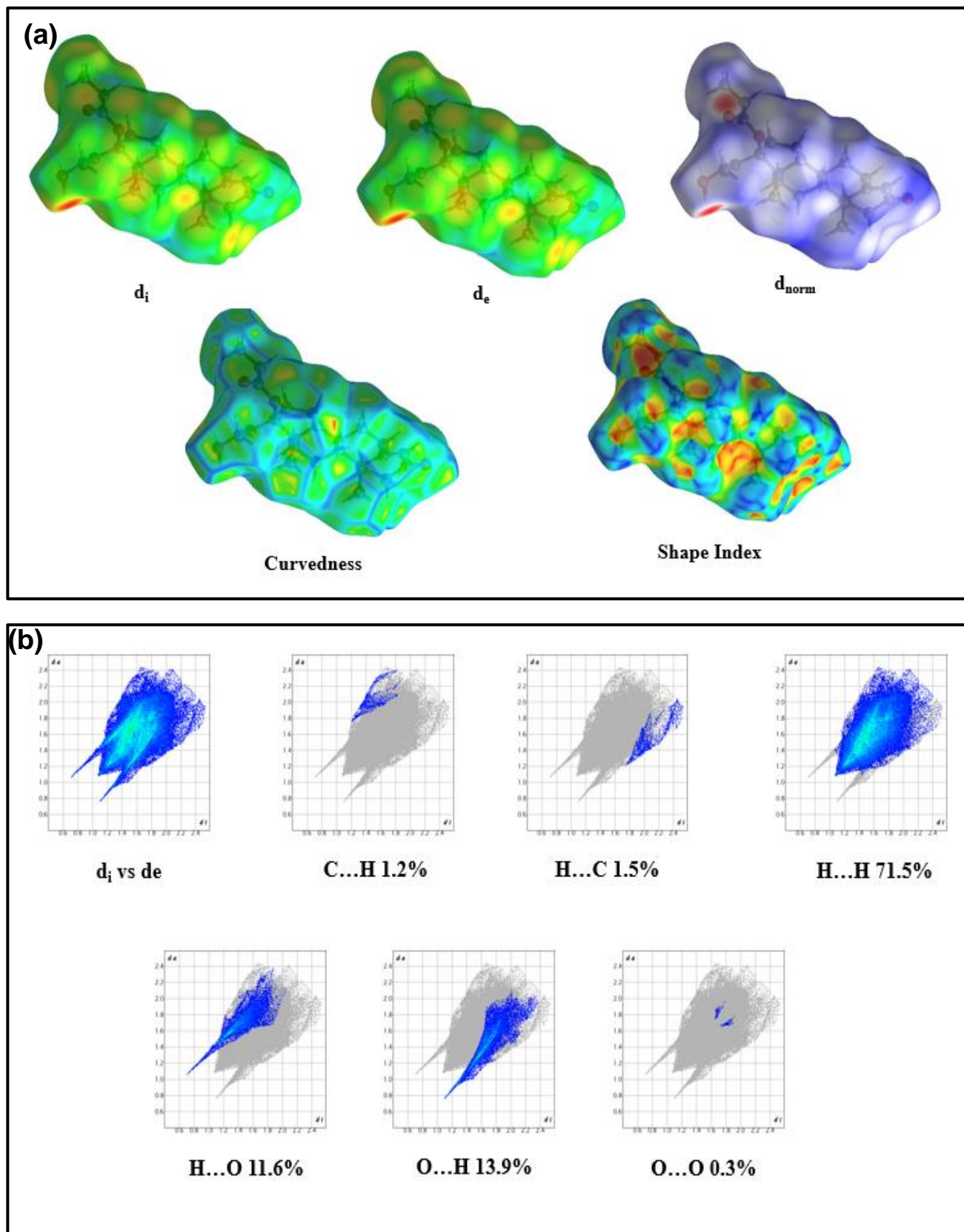
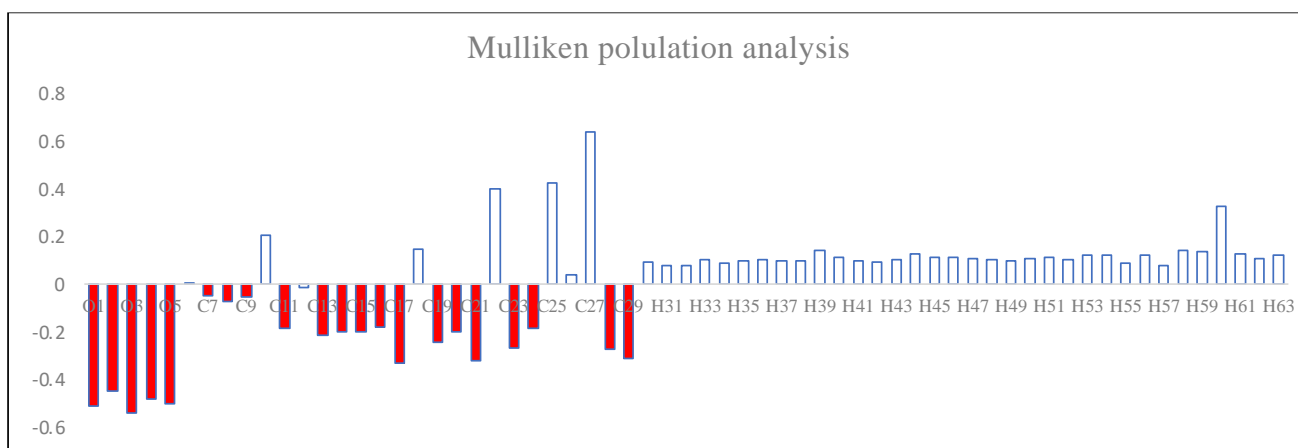


Table 6. Second order perturbation theory of Fock matrix in selected NBO basis for clascosterone

Donor (i)	Type	Acceptor (j)	Type	Type of transition	E(2) ^a (KJ/mol)	E(j)-E(i) ^b (a.u)	F(i,j) ^c (a.u)
C ₁₈ -C ₂₄	π	O ₄ -C ₂₅	π*	π- π*	21.77	0.29	0.072
O ₁	L(2)	O ₅ -C ₂₇	π*	L(2)- π*	45.53	0.32	0.109
O ₂	L(2)	C ₁₀ -C ₂₂	σ*	L(2)- σ*	19.85	0.63	0.101
O ₂	L(2)	C ₂₂ -C ₂₆	σ*	L(2)- σ*	19.76	0.63	0.101
O ₄	L(2)	C ₂₅ -C ₂₃	σ*	L(2)- σ*	20.12	0.64	0.102
O ₄	L(2)	C ₂₄ -C ₂₅	σ*	L(2)- σ*	18.22	0.71	0.103
O ₅	L(2)	O ₁ -C ₂₇	σ*	L(2)- σ*	29.52	0.62	0.122
O ₅	L(2)	C ₂₇ -C ₂₈	σ*	L(2)- σ*	17.43	0.66	0.098

**Figure 8.** Mulliken population analysis of clascosterone**Table 7.** Mulliken population analysis of clascosterone in the gas phase

Atom	Charges (e)	Atom	Charges (e)	Atom	Charges (e)
O ₁	-0.50843	C ₂₂	0.399064	H ₄₃	0.106015
O ₂	-0.44678	C ₂₃	-0.26853	H ₄₄	0.126133
O ₃	-0.54004	C ₂₄	-0.18158	H ₄₅	0.112552
O ₄	-0.4816	C ₂₅	0.42383	H ₄₆	0.114522
O ₅	-0.49809	C ₂₆	0.040861	H ₄₇	0.10626
C ₆	0.003544	C ₂₇	0.638068	H ₄₈	0.101446
C ₇	-0.04823	C ₂₈	-0.27309	H ₄₉	0.097718
C ₈	-0.06939	C ₂₉	-0.3121	H ₅₀	0.109673
C ₉	-0.05355	H ₃₀	0.091486	H ₅₁	0.111488
C ₁₀	0.206161	H ₃₁	0.078723	H ₅₂	0.105116
C ₁₁	-0.18447	H ₃₂	0.079891	H ₅₃	0.122279
C ₁₂	-0.01108	H ₃₃	0.105615	H ₅₄	0.124084
C ₁₃	-0.2103	H ₃₄	0.088255	H ₅₅	0.090975
C ₁₄	-0.19973	H ₃₅	0.098384	H ₅₆	0.123189
C ₁₅	-0.19778	H ₃₆	0.101519	H ₅₇	0.080502
C ₁₆	-0.18031	H ₃₇	0.099338	H ₅₈	0.140226

C ₁₇	-0.3299	H ₃₈	0.098846	H ₅₉	0.138766
C ₁₈	0.149161	H ₃₉	0.143693	H ₆₀	0.327364
C ₁₉	-0.24344	H ₄₀	0.112622	H ₆₁	0.129524
C ₂₀	-0.19738	H ₄₁	0.099146	H ₆₂	0.108083
C ₂₁	-0.31777	H ₄₂	0.095365	H ₆₃	0.124056

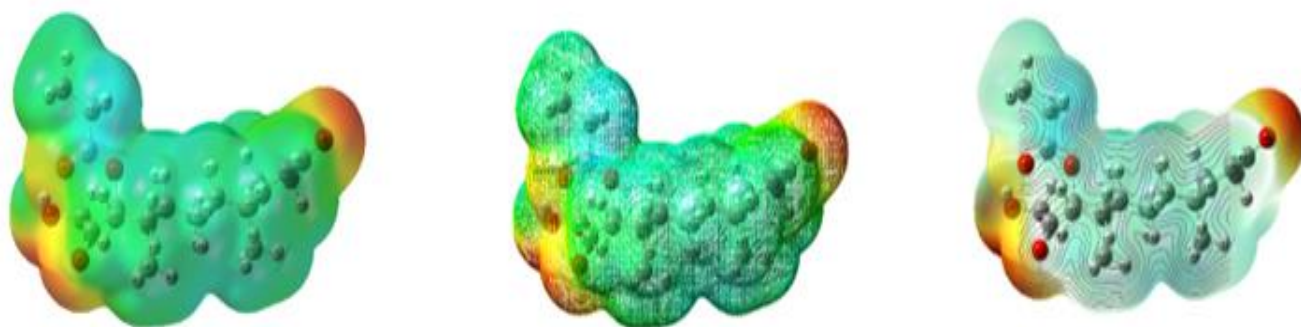


Figure 9. Total electron density and the contour map with molecular electrostatic potential surface of clascosterone

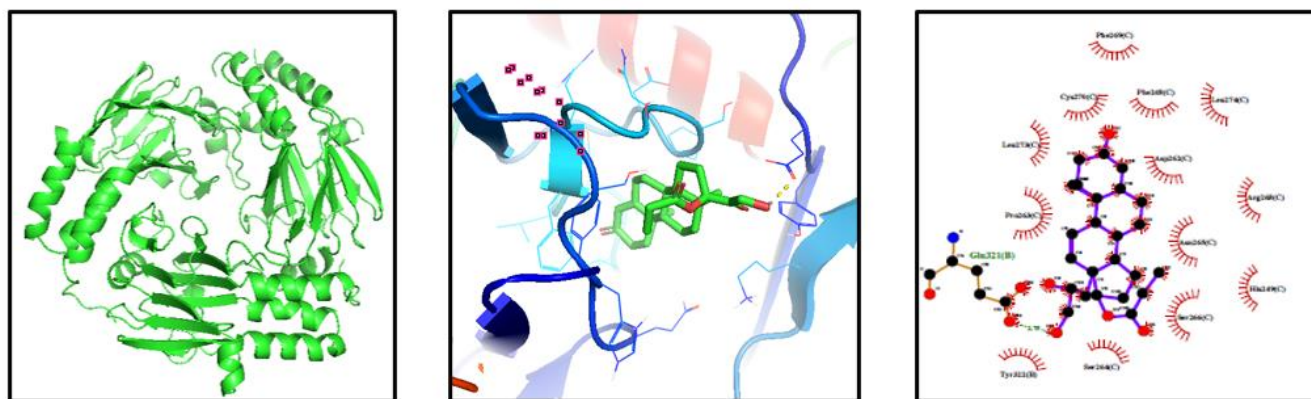


Figure 10. Molecular docking of clascosterone against SMAD3 protein

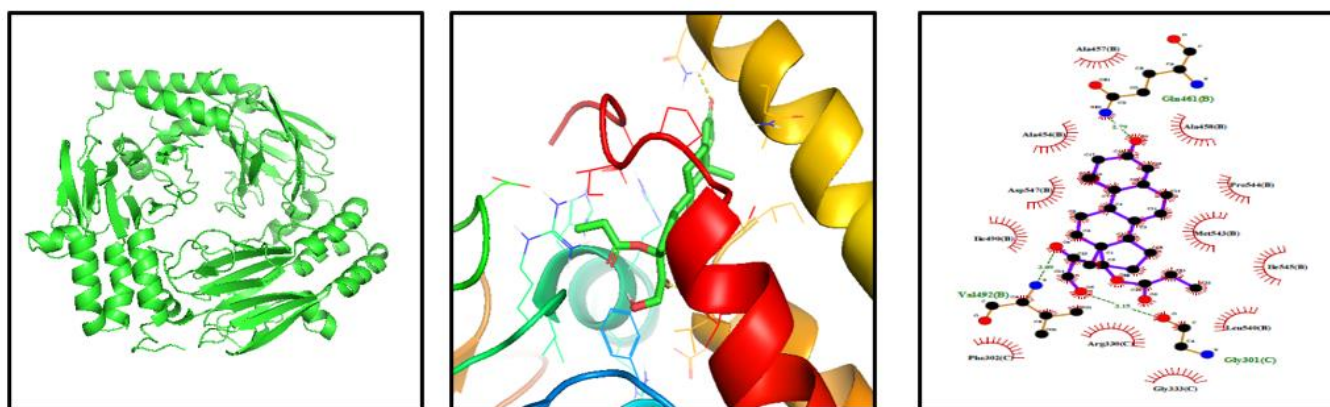


Figure 11. Molecular docking of clascosterone against SMAD4 protein

Table 8. Molecular docking studies of clascosterone against SMAD proteins

Proteins	Binding energy (Kcal/mol)	No. of hydrogen bonding	Amino acids	Bond length (Å)	Hydrophobic interaction
SMAD 3	-8.22	1	Glutamic acid 321	2.75	Phenylalanine 269, 248 Cystine 270 Leucine 273, 274 Aspartic acid 262 Proline 263 Arginine 268 Asparagine 265 Histidine 249 Serine 264, 266 Tyrosine 322
SMAD 4	-8.57	3	Alanine 457 Valine 492 Glycine 301	2.79 3.09 3.15	Alanine 454, 457, 458 Proline 544 Aspartic acid 547 Isoleucine 490, 545 Methionine 543 Leucine 540 Phenylalanine 302 Arginine 330 Glycine 333

3.9. Molecular docking

Molecular docking aids drug discovery by predicting the affinity between small molecules and target proteins before experimental testing [46-48]. The resolutions of the target proteins, labeled 1U7F and 1U7V in the Protein Data Bank (PDB), were 2.60 and 2.70 Å, respectively. Upon examining the interactions between the ligand clascosterone and the SMAD proteins (1U7F and 1U7V), nine conformations were produced, from which the conformation with the lowest binding energy was selected. The results of this investigation reveal binding energies of -8.22 and -8.57 kcal/mol for the interactions between clascosterone and SMAD3 and SMAD4, respectively. Additionally, the two-dimensional and three-dimensional interaction diagrams between the proteins and ligands are depicted in Figures 10 and 11, with an emphasis on significant polar (hydrophobic) and nonpolar (hydrogen bonding) interactions. The corresponding binding scores are provided in Table 8.

4. Conclusion

Computational methods were utilized to investigate various aspects of the molecular structure of

clascosterone, including geometrical parameters, spectroscopic features, donor-acceptor interactions, Hirshfeld surfaces, and ligand-protein interactions. Optimized geometric parameters closely align with experimental observations, and vibrational frequencies confirm the existence of CC, CH, C-O, C=O, CH₂, and CH₃ groups, providing evidence for the stable structure of clascosterone. The transition at 252 nm exhibits an excitation energy of 4.91 eV, while the DOS spectrum reveals an energy gap of 5.018 eV, with occupied orbitals shown in green and empty orbitals in red. Methine proton H55 experiences a higher chemical shift than other methine protons due to the neighbouring electronegative oxygen atom (O4), which deshields the electrons from H55. NBO analysis identifies the primary interaction energy originating from electron donation from O1 to O5-C27 via the L(2)→π* transition, stabilizing at 46.53 kJ/mol. Additionally, the Hirshfeld surface indicates that H•••H interactions (71.5%) predominate, followed by O•••H interactions (25.5%). The MEP map reveals red zones over OH and C=O groups, indicating an electron-rich site and suitable for electrophilic reactivity, while blue zones around hydrogen atoms in the ring and CH₃/CH₂ groups suggest low electron density and potential nucleophilic reactivity, consistent with Mulliken charge distribution. Lastly,

molecular docking of clascoterone against SMAD proteins SMAD 3 and SMAD 4 revealed substantial binding energies of -8.22 kcal/mol and -8.57 kcal/mol, respectively, suggesting its potential as an antitumor agent.

References

- [1] S.M. Tuchayi, E. Makrantonaki, R. Ganceviciene, C. Dessinioti, S.R. Feldman, C.C Zouboulis, Acne vulgaris. *Nature Reviews Disease primers*, 1(1), (2015) 1-20. <https://doi.org/10.1038/nrdp.2015.29>
- [2] D.D Lynn, T. Umari, C.A. Dunnick, R.P. Dellavalle, The epidemiology of acne vulgaris in late adolescence. *Adolescent health, medicine and therapeutics*, 7, (2016) 13-25. <https://doi.org/10.2147/AHMT.S55832>
- [3] J.K. Tan, K. Bhate, A global perspective on the epidemiology of acne. *British Journal of Dermatology*, 172(S1), (2015) 3-12. <https://doi.org/10.1111/bjd.13462>
- [4] J.Q. Del Rosso, L.H. Kircik, D. Thiboutot, Androgens, Androgen Receptors, and the Skin: From the Laboratory to the Clinic with Emphasis on Clinical and Therapeutic Implications. *Journal of drugs in dermatology: JDD*, 19(3), (2020) 30-35.
- [5] D. Dart, Androgens have forgotten and emerging roles outside of their reproductive functions, with implications for diseases and disorders. *Journal of Endocrine Disorders*, 1(1), (2014) 1005.
- [6] M.L. Elsaie, Hormonal treatment of acne vulgaris: an update. *Clinical, Cosmetic and Investigational Dermatology*, (9), (2016) 241-248. <https://doi.org/10.2147/CCID.S114830>
- [7] J.J. Lai, P. Chang, K.P. Lai, L. Chen, C. Chang, The role of androgen and androgen receptor in skin-related disorders. *Archives of dermatological research*, 304, (2012) 499-510. <https://doi.org/10.1007/s00403-012-1265-x>
- [8] A.M. Layton, E.A. Eady, H. Whitehouse, J.Q. Del Rosso, Z. Fedorowicz, E.J. van Zuuren, Oral spironolactone for acne vulgaris in adult females: a hybrid systematic review. *American journal of clinical dermatology*, 18 (2017) 169-191. <https://doi.org/10.1007/s40257-016-0245-x>
- [9] J.Q. Del Rosso, L.H. Kircik, D. Thiboutot, Androgens, Androgen Receptors, and the Skin: From the Laboratory to the Clinic with Emphasis on Clinical and Therapeutic Implications. *Journal of drugs in dermatology: JDD*, 19(3) (2020) 30-35.
- [10] L.H. Kircik, Androgens and acne: perspectives on clascoterone, the first topical androgen receptor antagonist. *Expert Opinion on Pharmacotherapy*, 22(13), (2021) 1801-1806. <https://doi.org/10.1080/14656566.2021.1918100>
- [11] L. Eichenfield, A. Hebert, L.S. Gold, M. Cartwright, E. Fragasso, L. Moro, A. Mazzetti, Open-label, long-term extension study to evaluate the safety of clascoterone (CB-03-01) cream, 1% twice daily, in patients with acne vulgaris. *Journal of the American Academy of Dermatology*, 83(2), (2020) 477-485. <https://doi.org/10.1016/j.jaad.2020.04.087>
- [12] S.T. Alkhoodaidi, K.A. Al Hawsawi, I.T. Alkhoodaidi, D. Magzoub, A. Abu-Zaid, Efficacy and safety of topical clascoterone cream for treatment of acne vulgaris: a systematic review and meta-analysis of randomized placebo-controlled trials. *Dermatologic Therapy*, 34(1) (2021) 14609. <https://doi.org/10.1111/dth.14609>
- [13] P. Ferraboschi, L. Legnani, G. Celasco, L. Moro, L. Ragonesi, D. Colombo, A full conformational characterization of antiandrogen cortexolone-17 α -propionate and related compounds through theoretical calculations and nuclear magnetic resonance spectroscopy. *MedChemComm*, 5(7), (2024) 904-914. <https://doi.org/10.1039/C4MD00049H>
- [14] A. Mazzetti, L. Moro, M. Gerloni, M. Cartwright, Pharmacokinetic profile, safety, and tolerability of clascoterone (cortexolone 17-alpha propionate, CB-03-01) topical cream, 1% in subjects with acne vulgaris: an open-label phase 2a study. *Journal of drugs in dermatology: JDD*, 18(6), (2019) 563-563.
- [15] A. Hebert, D. Thiboutot, L.S. Gold, M. Cartwright, M. Gerloni, E. Fragasso, A. Mazzetti, Efficacy and safety of topical clascoterone cream, 1%, for treatment in patients with facial acne: two phase 3 randomized clinical trials. *JAMA dermatology*, 156(6), (2020) 621-630. <https://doi.org/10.1001/jamadermatol.2020.0465>
- [16] C. Rosette, N. Rosette, A. Mazzetti, L. Moro, M. Gerloni, Cortexolone 17 α -propionate (clascoterone) is an androgen receptor antagonist in dermal papilla cells in vitro. *Journal of drugs in dermatology: JDD*, 18(2), (2019) 197-201.
- [17] H.Y. Sun, D.F. Sebaratnam, Clascoterone as a novel treatment for androgenetic alopecia. *Clinical and Experimental Dermatology*, 45(7), (2020) 913-914. <https://doi.org/10.1111/ced.14292>
- [18] A. Hargis, M. Yaghi, N.M. Bermudez, H. Lev-Tov, Clascoterone in the treatment of mild hidradenitis suppurativa. *Journal of the American Academy of Dermatology*, 90(1), (2024) 142-144. <https://doi.org/10.1016/j.jaad.2023.08.064>
- [19] A. Ram Kumar, C. Senthamil Selvi, S. Selvaraj, G.P. Sheeja Mol, P. Jayaprakash, In silico

- studies on the molecular geometry, FMO, Mulliken charges, MESP, ADME and molecular docking prediction of pyrogallol carboxaldehydes as potential anti-tumour agents, *Phys. Chem. Res.* 12(2), (2024) 305-320. <https://doi.org/10.22036/PCR.2023.402835.2359>
- [20] A. Ram Kumar, S. Selvaraj, P. Anthoniammal, R.J. Ramalingam, B. Ranjith, P. Jayaprakash, G.P. Sheeja Mol, Comparison of spectroscopic, structural, and molecular docking studies of 5-nitro-2-fluoroaniline and 2-nitro-5-fluoroaniline: An attempt on fluoroaniline isomers, *Journal of Fluorine Chemistry*, 270, (2023) 110167. <https://doi.org/10.1016/j.jfluchem.2023.110167>
- [21] W. Kohn, L.J. Sham, Self-consistent equations including exchange and correlation effects. *Physical Review Journals Archive*, 140, (1965) A1133–A1138. <https://doi.org/10.1103/PhysRev.140.A1133>
- [22] A.D. Becke, Density functional thermo chemistry – I: the effect of the exchange only gradient correlation, *Journal of Chemical Physics*, 98, (1993) 5648–5652. <https://doi.org/10.1063/1.462066>
- [23] C. Lee, W. Yang, R.G. Parr, Development of the Colle-Salvetti correlation-energy formula into a functional of the electron density, *Physical Review B*, 37, (1988) 785–789.
- [24] W.J. Hehre, R. Ditchfield, J.A. Pople, Self-consistent molecular orbital methods. XII. Further extensions of Gaussian-type basis sets for use in molecular orbital studies of organic molecules. *The Journal of Chemical Physics*, 56(5), (1972) 2257–2261. <https://doi.org/10.1103/PhysRevB.37.785>
- [25] J.R. Cheeseman, G.W. Trucks, T.A. Keith, M.J. Frisch, A comparison of models for calculating nuclear magnetic resonance shielding tensors. *The Journal of Chemical Physics*, 104 (1996) 5497–5509, <https://doi.org/10.1063/1.471789>
- [26] M. Petersilka, U.J. Gossmann, E.K.U. Gross, Excitation energies from time-dependent density-functional theory. *Physical Review Letters*, 76, (1996) 1212–1215. <https://doi.org/10.1103/PhysRevLett.76.1212>
- [27] E. Runge, E.K.U. Gross, Density functional theory for time-dependent systems. *Physical Review Letters*, 52, (1984) 997. <https://doi.org/10.1103/PhysRevLett.52.997>
- [28] G.A. Zhurko, D.A. Zhurko, Chemcraft program version 1.6 (Build 315), (2009) <http://www.chemcraftprog.com>
- [29] S.K. Wolff, D.J. Grimwood, J.J. McKinnon, M.J. Turner, D. Jayatilaka, M.A. Spackman, (2012) *Crystal Explorer (Version 3.1)*, University of Western Australia.
- [30] G.M. Morris, R. Huey, W. Lindstrom, M.F. Sanner, R.K. Belew, D.S. Goodsell, A.J. Olson, AutoDock4 and AutoDockTools4: Automated docking with selective receptor flexibility. *Journal of computational chemistry*, 30(16), (2009) 2785-2791. <https://doi.org/10.1002/jcc.21256>
- [31] W.L. DeLano, Pymol: an open-source molecular graphics tool. *CCP4 Newsletter on protein Crystallography*, 40(1), (2002) 82–92. <http://www.pymol.org>
- [32] A.C. Wallace, R.A. Laskowski, J.M. Thornton, LIGPLOT: a program to generate schematic diagrams of protein–ligand interactions. *Protein Engineering, Design and Selection*, 8(2), (1995) 127-134. <https://doi.org/10.1093/protein/8.2.127>
- [33] P. Ferraboschi, M.C. Sala, R. Stradi, L. Ragonesi, C. Gagliardi, P. Lanzarotti, E.M. Ragg, F. Meneghetti, Full spectroscopic characterization of two crystal pseudopolymorphic forms of the antiandrogen corticosterone 17 α -propionate for topical application. *Steroids*, 128, (2017) 95-104. <https://dx.doi.org/10.5517/ccdc.csd.cc1144f9>
- [34] A. Ram Kumar, N. Kanagathara, Spectroscopic, structural and molecular docking studies on N, N-dimethyl-2-[6-methyl-2-(4-methylphenyl) imidazo [1, 2-a] pyridin-3-yl] acetamide. *Physical Chemistry Research*, 12(1), (2024) 95-107. <https://doi.org/10.22036/PCR.2023.387911.2306>
- [35] A. Ram Kumar, S. Selvaraj, K.S. Jayaprakash, S. Gunasekaran, S. Kumaresan, J. Devanathan, K.A. Selvam, L. Ramadass, M. Mani, P. Rajkumar, Multi-spectroscopic (FT-IR, FT-Raman, ¹H NMR and ¹³C NMR) investigations on syringaldehyde. *Journal of Molecular Structure*, 1229, (2021) 129490. <https://doi.org/10.1016/j.molstruc.2020.129490>
- [36] A. Ram Kumar, S. Selvaraj, M. Azam, G.P. Sheeja Mol, N. Kanagathara, M. Alam, P. Jayaprakash, Spectroscopic, biological, and topological insights on lemonol as a potential anticancer agent. *ACS Omega*, 8(34), (2023) 31548-31566. <https://doi.org/10.1021/acsomega.3c04922>
- [37] S. Selvaraj, A. Ram Kumar, T. Ahilan, M. Kesavan, G. Serdaroglu, P. Rajkumar, M. Mani, S. Gunasekaran, S. Kumaresan, Experimental and Theoretical Spectroscopic Studies of the Electronic Structure of 2-Ethyl-2-phenylmalonamide. *Physical Chemistry Research*, 10(3), (2022) 333-344.
- [38] S. Selvaraj, A. Ram Kumar, T. Ahilan, M. Kesavan, S. Gunasekaran, S. Kumaresan, Multi spectroscopic and computational investigations on the electronic structure of oxyclozanide. *Journal of the Indian Chemical Society*, 99(10),

- (2022) 100676.
<https://doi.org/10.1016/j.jics.2022.100676>
- [39] A. Ram Kumar, S. Selvaraj, P. Rajkumar, J. Dhanalakshmi, M. Kumar, S.K. Nagarajan, P. Jayaprakash, G.P.S. Mol, S. Awasthi, S.K. Pandey, Insights into structural, vibrational, and chemical shift characteristics, solvents impact (polar and nonpolar) on electronic properties and reactive sites, ADMET predictions, and ligand-protein interactions for antiviral drugs safrrole and isosafrole: An in-silico approach. *Chemical Physics Impact*, 8, (2023) 100443. <https://doi.org/10.1016/j.chphi.2023.100443>
- [40] K. Thirunavukkarasu, P. Rajkumar, S. Selvaraj, R. Suganya, M. Kesavan, S. Gunasekaran, S. Kumaresan, Vibrational (FT-IR and FT-Raman), electronic (UV-Vis), NMR (¹H and ¹³C) spectra and molecular docking analyses of anticancer molecule 4-hydroxy-3-methoxycinnamaldehyde. *Journal of Molecular Structure*, 1173, (2018) 307-320. <https://doi.org/10.1016/j.molstruc.2018.07.003>
- [41] S. Premkumar, A. Jawahar, T. Mathavan, M. Kumara Dhas, V.G. Sathe, A. Milton Franklin Benial, DFT calculation and vibrational spectroscopic studies of 2-(tert-butoxycarbonyl (Boc)-amino)-5-bromopyridin. *Spectrochimica Acta Part A: Molecular and Biomolecular Spectroscopy*, 129, (2014) 74-83. <https://doi.org/10.1016/j.saa.2014.02.147>
- [42] P. Rajkumar, S. Selvaraj, R. Suganya, M. Kesavan, G. Serdaroglu, S. Gunasekaran, S. Kumaresan, Experimental and theoretical investigations on electronic structure of 5-(hydroxymethyl)-2-furaldehyde: An antisickling agent identified from terminalia bellirica. *Chemical Data Collections*, 29, (2020) 100498, <https://doi.org/10.1016/j.cdc.2020.100498>
- [43] M.U. Hasan, M.F. Ali, A. Bukhari, Structural characterization of Saudi Arabian heavy crude oil by nmr spectroscopy, *Fuel*. 62(5), (1983) 518-523 [https://doi.org/10.1016/0016-2361\(83\)90219-3](https://doi.org/10.1016/0016-2361(83)90219-3)
- [44] Fiorella Meneghetti CCDC 1463711: Experimental Crystal Structure Determination, 2016, <https://doi.org/10.5517/ccdc.csd.cc1143hb>
- [45] A. Ram Kumar, S. Selvaraj, G. Sheeja Mol, M. Selvaraj, L. Ilavarasan, S.K. Pandey, P. Jayaprakash, S. Awasthi, O. Albormani, A. Ravi, Synthesis, solvent-solute interactions (polar and nonpolar), spectroscopic insights, topological aspects, Fukui functions, molecular docking, ADME, and donor-acceptor investigations of 2-(trifluoromethyl) benzimidazole: A promising candidate for antitumor pharmacotherapy. *Journal of Molecular Liquids*, 393, (2023) 123661. <https://doi.org/10.1016/j.molliq.2023.123661>.
- [46] A. Ram Kumar, L. Ilavarasan, G. Sheeja Mol, S. Selvaraj, M. Azam, P. Jayaprakash, M. Kesavan, M. Alam, J. Dhanalakshmi, S.I. Al-Resayes, A. Ravi, Spectroscopic (FT-IR, FT-Raman, UV-Vis and NMR) and computational (DFT, MESP, NBO, NCI, LOL, ELF, RDG and QTAIM) profiling of 5-chloro-2-hydroxy-3-methoxybenzaldehyde: A promising antitumor agent. *Journal of Molecular Structure*, 1298, (2023) 136974, <https://doi.org/10.1016/j.molstruc.2023.136974>
- [47] S. Selvaraj, Computational study on the structural features, vibrational aspects, chemical shifts, and electronic properties of 1, 4- Dinitrosopiperazine-2-carboxylic acid: Insights into donor-acceptor interactions and thermodynamic properties. *International Research Journal of Multidisciplinary Technovation*, 6(1), (2024) 1-16. <https://doi.org/10.54392/irjmt2411>
- [48] P. Rajkumar, S. Selvaraj, P. Anthoniammal, A. Ram Kumar, K. Kasthuri, S. Kumaresan, S., 2023. Structural (monomer and dimer), spectroscopic (FT-IR, FT-Raman, UV-Vis and NMR) and solvent effect (polar and nonpolar) studies of 2-methoxy-4-vinyl phenol. *Chemical Physics Impact*, 7, (2023) 100257, <https://doi.org/10.1016/j.chphi.2023.100257>

Authors Contribution Statement

C. Karnan – Writing - Review & Editing, Visualization and Validation. A. Ram Kumar – Writing - Original draft, Methodology, Data Analysis. S. Selvaraj – Writing - Review & Editing, Conceptualization and Supervision.

Funding

The research was carried out without the aid of any financial grants.

Competing Interests

The authors declare that there are no conflicts of interest regarding the publication of this manuscript.

Data Availability

The data supporting the findings of this study can be obtained from the corresponding author upon reasonable request.

Has this article screened for similarity?

Yes

About the License

© The Author(s) 2024. The text of this article is open access and licensed under a Creative Commons Attribution 4.0 International License.